

Rainfall as a Driver for Near-Surface Turbulence and Air-Water Gas Exchange in Aquatic Systems

Eliana Bohórquez-Bedoya¹, Lorenzo Rovelli², and Andreas Lorke³

¹Universidad Nacional de Colombia

²Universität Koblenz-Landau

³University of Koblenz and Landau

November 24, 2022

Abstract

Gas exchange at air-water interfaces is regulated by near-surface turbulence and can be controlled by different atmospheric forcing conditions, with wind speed and surface buoyancy flux being the most recognized drivers in empirical studies and modeling approaches. The effect of rainfall on near-surface turbulence has rarely been studied and a consistent relationship between rain rate and near-surface turbulence has not yet been established. In this study, we explore the influence of rain on near-surface turbulence and gas transfer velocities over a wide range of rain rates (7 to 90 mm h⁻¹) under laboratory conditions, using particle image velocimetry measurements and dissolved oxygen as a gas tracer. The rain-induced dissipation rates of turbulent kinetic energy declined with depth following a consistent power-law relationship. Both energy dissipation rates and gas transfer velocity increased systematically with the rainfall rate. The results confirm the causal relationships between rainfall, turbulence, and gas exchange. In addition, we propose a power-law relationship between near-surface turbulent dissipation rates and rain rate. In combination with surface renewal theory, we derived a direct relationship between gas transfer velocity and rain rate, which can be used to assess the importance of short-term drivers, such as rain events, on gas dynamics and biogeochemical cycling in aquatic ecosystems.

Hosted file

essoar.10509986.1.docx available at <https://authorea.com/users/549215/articles/603400-rainfall-as-a-driver-for-near-surface-turbulence-and-air-water-gas-exchange-in-aquatic-systems>

Table 1. Summary of experimental results. R is the rain rate, T is the water temperature and Sc_{O_2} is the Schmidt number of oxygen at temperature T . ϵ_{Back} , ϵ_{Total} and ϵ_{Rain} are the background (estimated during no-rain periods), the total (estimated during rain), and the rain-induced turbulent dissipation rates, respectively, estimated at 6.5 cm depth. k_{600_Back} , k_{600} and k_{600_mod} are the background (estimated during no rain periods), total (estimated during rain) and the model-predicted gas transfer velocities (equation (15)), respectively. F_{KE} is the estimated kinetic energy flux of rain. Note that ϵ_{Back} and ϵ_{Rain} for rain rates of 10.3 and 13.5 mm h⁻¹ could not be determined (ND) due to poor video quality in the measurements without rain.

Run	R [mm h ⁻¹]	T [°C]	Sc_{O_2}	ϵ_{Back} [W kg ⁻¹]	ϵ_{Total} [W kg ⁻¹]	ϵ_{Rain} [W kg ⁻¹]	$\frac{\epsilon_{Rain}}{\epsilon_{Total}}$	k_{600_Back} [cm h ⁻¹]	k_{600} [cm h ⁻¹]	k_{600_mod} [cm h ⁻¹]	F_{KE} [W m ⁻²]
1	6.90	16.9 ± 0.054	623	1.3 × 10 ⁻⁸	2.4 × 10 ⁻⁸	1.1 × 10 ⁻⁸	44%	0.820	2.99	11.2	0.0667
2	8.05	17.1 ± 0.055	615	1.3 × 10 ⁻⁸	3.0 × 10 ⁻⁸	1.6 × 10 ⁻⁸	55%	0.820	6.97	12.0	0.0775
3	10.3	9.48 ± 0.030	927	ND	3.2 × 10 ⁻⁸	ND	ND	-0.058	8.29	14.4	0.0992
4	13.5	9.35 ± 0.027	933	ND	8.1 × 10 ⁻⁸	ND	ND	-0.058	22.0	16.5	0.130
5	16.0	9.13 ± 0.737	945	1.1 × 10 ⁻⁸	1.1 × 10 ⁻⁷	9.5 × 10 ^{-8*}	90%	4.295	48.2*	18.0	0.154
6	16.2	8.59 ± 0.020	973	5.8 × 10 ⁻⁹	1.0 × 10 ⁻⁷	2.5 × 10 ⁻⁸	81%	0.202	28.2	20.8	0.211
7	21.1	8.36 ± 0.016	979	5.8 × 10 ⁻⁹	3.0 × 10 ⁻⁸	9.8 × 10 ⁻⁸	94%	0.202	15.6	18.2	0.168
8	19.8	8.49 ± 0.021	986	5.8 × 10 ⁻⁹	2.4 × 10 ⁻⁷	2.3 × 10 ⁻⁷	98%	0.202	16.7	20.1	0.227
9	25.0	16.8 ± 0.062	624	7.5 × 10 ⁻⁹	7.6 × 10 ⁻⁸	6.8 × 10 ⁻⁸	90%	-0.639	18.0	21.4	0.241
10	26.0	11.0 ± 0.010	852	6.9 × 10 ⁻⁹	7.6 × 10 ⁻⁸	6.9 × 10 ⁻⁸	91%	3.632	25.6	22.7	0.250
11	28.8	17.4 ± 0.087	607	7.5 × 10 ⁻⁹	9.8 × 10 ⁻⁸	9.1 × 10 ⁻⁸	92%	-0.639	19.3	22.9	0.277
12	39.4	11.1 ± 0.013	849	6.9 × 10 ⁻⁹	3.1 × 10 ⁻⁷	3.1 × 10 ⁻⁷	98%	3.632	30.3	28.0	0.380
13	48.9	17.8 ± 0.146	593	7.5 × 10 ⁻⁹	2.7 × 10 ⁻⁷	2.6 × 10 ⁻⁷	97%	-0.639	25.3	29.9	0.471
14	88.9	18.5 ± 0.220	572	7.5 × 10 ⁻⁹	3.8 × 10 ⁻⁷	3.7 × 10 ⁻⁷	98%	-0.639	46.5	40.3	0.856

* marks an outlier that caused the run with 16 mm h⁻¹ to be excluded from the subsequent analysis

Eliana Bohórquez-Bedoya^{1,2,*}, Lorenzo Rovelli², and Andreas Lorke²

¹ Department of Geosciences and Environment, Universidad Nacional de Colombia, Medellín, Colombia.

² Institute for Environmental Sciences, University of Koblenz-Landau, Landau, Germany.

* Corresponding author: Eliana Bohórquez-Bedoya (elibohorquezbed@unal.edu.co)

Key Points:

- Rain systematically enhances the gas transfer velocity at the air-water interface
- Near-surface turbulence can be expressed as a function of rain rate
- Surface renewal model is well suited to describe the effect of the rain rate on gas transfer velocity

Abstract

Gas exchange at air-water interfaces is regulated by near-surface turbulence and can be controlled by different atmospheric forcing conditions, with wind speed and surface buoyancy flux being the most recognized drivers in empirical studies and modeling approaches. The effect of rainfall on near-surface turbulence has rarely been studied and a consistent relationship between rain rate and near-surface turbulence has not yet been established. In this study, we explore the influence of rain on near-surface turbulence and gas transfer velocities over a wide range of rain rates (7 to 90 mm h⁻¹) under laboratory conditions, using particle image velocimetry measurements and dissolved oxygen as a gas tracer. The rain-induced dissipation rates of turbulent kinetic energy declined with depth following a consistent power-law relationship. Both energy dissipation rates and gas transfer velocity increased systematically with the rainfall rate. The results confirm the causal relationships between rainfall, turbulence, and gas exchange. In addition, we propose a power-law relationship between near-surface turbulent dissipation rates and rain rate. In combination with surface renewal theory, we derived a direct relationship between gas transfer velocity and rain rate, which can be used to assess the importance of short-term drivers, such as rain events, on gas dynamics and biogeochemical cycling in aquatic ecosystems.

Plain Language Summary

Gas exchange between the atmosphere and the water surface is regulated by turbulence at the water surface, which in turn is affected by atmospheric conditions. Rainfall rate has not been widely studied as a mechanism for the generation of near-surface turbulence in aquatic systems. In this study, we used a wide range of rainfall rates in laboratory experiments to understand the influence of rainfall on near-surface turbulence and gas transfer velocity. Turbulence estimates were based on videos resolving movement of particles in the water, and changes

in dissolved oxygen concentration in water were used to estimate gas transfer velocities. The results confirmed the causal relationships between rainfall, turbulence, and gas transfer velocity and revealed systematic relationships for turbulence and gas transfer velocity as functions of rainfall rate. We propose a power-law relationship between turbulence and rainfall rate. In addition, using a theoretical framework for relating turbulence and gas transfer velocity (known as surface renewal theory), we derive a direct relationship between gas transfer velocity and rainfall rate. These results can be used to evaluate the impact of rainfall on gas dynamics and biogeochemical cycles in aquatic ecosystems, topics of general interest in the context of climate change.

1 Introduction

Rainfall plays a fundamental role in the biosphere, e.g., in climate, hydrological, and biogeochemical cycles (Schlesinger & Bernhardt, 2013; Winter, 2004). On water surfaces, rainfall also causes physical impacts (Rooney et al., 2018) that affect, among other processes, the gas exchange across the air-water interface in the ocean (Turk et al., 2010), in lakes, and in reservoirs (Gu erin et al., 2007a; Ojala et al., 2011). Air-water gas exchange has important implications in aquatic ecosystems and in the global biogeochemical cycles of climatically important gases (Ho et al., 2018; Raymond et al., 2013), e.g. CO₂ uptake of the ocean and greenhouse gas emissions from inland waters (Cole & Caraco, 1998; Zappa et al., 2009). Currently, the prediction of gas exchange rates and their dependence on variable and dynamic environmental conditions are among the major uncertainties in existing models and interpretation of empirical data (Harrison & Veron, 2017; Rantakari et al., 2015).

The transport of gases across an air-water interface is commonly described as a diffusive flux that can be parameterized as the product of the gas transfer velocity (K) and the difference between dissolved gas concentration at the water surface and the atmospheric equilibrium concentration. The magnitude of K is related to near-surface turbulence at the water-side of the interface (Katul & Liu, 2017; Lamont & Scott, 1970) and controlled by different hydrodynamic forcing mechanisms, most of them hydrometeorological in nature (Guseva et al., 2021; Zappa et al., 2007). Traditionally, K has been estimated as a function of wind speed through empirical models (Cole & Caraco, 1998; Ho et al., 2007; Wanninkhof, 1992), and surface buoyancy flux during convective cooling (Poindexter et al., 2016; Read et al., 2012). Other processes that affect the exchange of gases and near-surface turbulence, such as rainfall, are mostly overlooked, although they may play an important role in gas exchange (Turk et al., 2010).

At the mechanistic level, the surface renewal theory (Lamont & Scott, 1970) provides a scaling relationship for gas transfer velocity based on near-surface turbulence, which led to a universal relationship between the gas transfer velocity and the dissipation rate of turbulent kinetic energy near the water surface (Katul & Liu, 2017; Lorke & Peeters, 2006). The surface renewal model has been validated for a wide range of environmental forcing conditions (Zappa et al., 2007).

Field studies in lakes and reservoirs at different latitudes have shown that rainfall events can have a strong impact on the gas transfer velocity (Gu erin et al., 2007b; Ojala et al., 2011). Laboratory studies have found that rainfall significantly enhances (by a factor of 3 to 40) the air-water gas exchange, especially at low to moderate wind speed (Harrison et al., 2012; Ho et al., 1997, 2000, 2004, 2007; Zappa et al., 2009). Ho et al. (2004) concluded that turbulence is the main mechanism affecting during rainfall events and growing evidence suggests that rainfall significantly increases near-surface turbulence in marine (Ho et al., 2004; Zappa et al., 2009) and freshwater (Harrison & Veron, 2017) environments.

To date, the available database on rain-generated turbulence is limited to a few studies and a narrow range of rainfall rates, making it difficult to establish a consistent relationship between turbulence and rain rate that could be generalized in biogeochemical models. Furthermore, there is no general consensus on the importance of rainfall for near-surface turbulence, as some studies have not found a significant contribution of rainfall on measured dissipation rates of turbulent kinetic energy (Bey a et al., 2011; Peirson et al., 2013).

When using rain rate as a scaling parameter, a major source of uncertainty comes from the distribution and heterogeneity of raindrop sizes and fall velocities. The assessment of such heterogeneity in both laboratory and natural conditions requires complex and extensive measurement (Zappa et al., 2009). Depending on drop size, raindrops reach their terminal fall velocity after a free-fall distance of ~20 m (Serio et al., 2019), which challenges laboratory setups. However, several studies have also shown that rain-induced air-water gas transfer is correlated to the kinetic energy flux of the rain (F_{KE}) (Ho et al., 1997, 2000, 2004; Zappa et al., 2009), which removes possible uncertainties related to drop sizes and fall velocities (Ho et al., 1997).

As it is challenging to characterize rain-induced turbulence under field conditions, where additional forcing mechanisms, such as wind, often prevail, experimental studies under controlled conditions are an ideal approach for this purpose. Quantitative experimental studies investigating rain-induced turbulence, however, remain scarce (Harrison & Veron, 2017). In former laboratory studies, gas transfer velocities during rainfall have mainly been estimated based on mass balances of trace gases, such as sulfur hexafluoride (SF_6), helium (He), nitrous oxide (N_2O), and carbon dioxide (CO_2) (Harrison et al., 2012; Harrison & Veron, 2017; Ho et al., 1997, 2000, 2004, 2007; Takagaki & Komori, 2007). Dissolved oxygen (O_2) has not yet been used as a gas tracer, despite the fact that it can be easily and cost-effectively manipulated and measured at high frequency.

Rain-induced turbulence has been typically characterized via high-resolution spatial mapping of turbulent flow velocities near the water surface (Harrison & Veron, 2017; Takagaki & Komori, 2007; Thielicke & Sonntag, 2021; Zappa et al., 2009), or single-point velocity observations at a fixed depth (Bey a et al., 2011; Harrison et al., 2012). Spatially-resolved observations of turbulent flow fields are facilitated by particle image velocimetry (PIV) measurements, which

have become an affordable, high-resolution technique in laboratory studies due to the advances in camera technology, computer power and the availability of open-source software for processing (Käufer et al., 2021; Thielicke & Sonntag, 2021). However, this technique has been mostly unexplored in the study of rain-induced turbulence. Harrison and Veron (2017) performed PIV measurements to gain a physical understanding of rain-induced turbulence. Their setup, however, focused on high rain rates (40, 100 and 190 mm h⁻¹), and thus did not cover the wide range of rain rates that occurs under environmental conditions.

The objective of this study is to analyze the effect of rain rate on near-surface turbulence and on the resulting gas transfer velocity and to elucidate empirical and mechanistic relationships between the gas transfer velocity and near-surface turbulence in dependence on rain rate and kinetic energy flux. We performed controlled laboratory experiments over a wide range of rain rates (7 to 90 mm h⁻¹) and estimated gas transfer velocities from high-resolution measurements of O₂ concentration, while rain-induced turbulence was characterized on the basis of PIV measurements. The general applicability of the observed relationship between gas transfer velocity and rain intensity is discussed in the context of surface renewal theory and previous empirical studies.

2 Materials and Methods

2.1 Experimental setup

Our experimental setup consisted of a custom-build rain generator, which was mounted ~20 m above a rain-collecting aquarium (Figure 1). To exclude effects of wind and solar radiation, the experiments were conducted in a closed tower (a hose-drying tower of a local fire brigade, Figure S1). Before each experimental series, the dissolved oxygen (O₂) concentration in the aquarium water was reduced to about 50% of its atmospheric equilibrium concentration. During experiments with varying rainfall intensity, we observed the reaeration rate of the water using an oxygen mass balance, as well as the turbulent velocity fields near the water surface (Figure 1). Additional measurements included rainfall rates and the size and fall velocity of raindrops.

The rain generator consisted of a frame (1 × 1 × 0.05 m) with a perforated plexiglas plate (3 mm of thickness). The footprint of the rain generator exceeded the surface area of the aquarium at all sides, ensuring a homogenous distribution of rain at the water surface. The plate had 580 holes with a diameter of 0.8 mm and with a regular spacing. The rain rate was varied by i) controlling the water level above the plate, and ii) by changing the number and size of open holes in the plate. The rain generator was manually fed with water stored at ambient temperature in an open tank. By varying the water level, we modified the frequency of drop formation at each hole, with a higher level resulting in a higher frequency of droplets and a higher overall rain rate. Some holes were closed with adhesive tape, and subsequently reopened by piercing the tape with a needle (0.4 mm diameter) or by removing the tape to revert to the original hole size. Open and closed holes were always homogeneously distributed across

the plate (Figure S2). During the experiments, we adjusted the number of open holes to target a range of rainfall rates between 5 and 90 mm h⁻¹, which correspond to the most frequent rainfall rates observed at a tropical freshwater reservoir (Figure S3).

2.2 Measurements and experiments

The aquarium that received the rain water had a volume of 125 L (50 × 50 × 50 cm) and was initially filled to a height of ~42 cm. The instrumental setup inside and outside of the aquarium facilitated estimating the gas transfer velocity, turbulent energy dissipation rates in water, and the rain rate (Figure 1).

Each experimental series of measurements consisted of a 15 min period without rain, followed by several 15 min runs with constant rain rates (rain periods). During the different runs, we maintained the same configuration (size and number of open holes), but varied the water level in the rainfall generator. Rain rates (R in mm h⁻¹) were estimated for each run as the mean rate of change of the water level in the aquarium, which was monitored using a high-resolution pressure probe (Duet, RBR Inc., sampling at 16 Hz).

For estimating gas transfer velocities, we monitored dissolved oxygen concentration in water with four fiber-optic sensors (FireStingO2, PyroScience GmbH), distributed vertically at 3, 13, 23 and 33 cm depth from the water surface. The sensors measured at a frequency of 1 Hz during the 15 min experimental runs. The water temperature and atmospheric pressure (P_{atm}) were measured at the same frequency.

To visualize the turbulent flow field, seeding particles (polyamid, 20 μm diameter) were added to the water in the aquarium and illuminated with a laser light sheet. We used a green (532 nm), continuous-wave, line laser (450 mW; Inline HP, MediaLas Electronics GmbH) to illuminate a vertical plane in the center of the aquarium. The dynamic distribution of the light scattering seeding particles was observed by recording videos with a consumer-grade camera (GoPro Hero4, GoPro Inc.) located at ~13 cm from the front face of the aquarium, with a frame rate of 30 fps and a resolution of 1920 × 1080 pixels. The field of view covered an area of 21 × 8 cm below the water surface and a portion of the air side of 3.5 cm height (Figure 1). Particle Image Velocimetry (PIV) measurements were performed for 3 min during each run. Additional measurements were made without rain at the beginning of each experimental series, to characterize background turbulence levels. For metric calibration of the videos, a short (~3 s) video was recorded prior to each series while placing a calibration target (0.5 × 0.5 cm checkerboard pattern) in the laser light sheet.

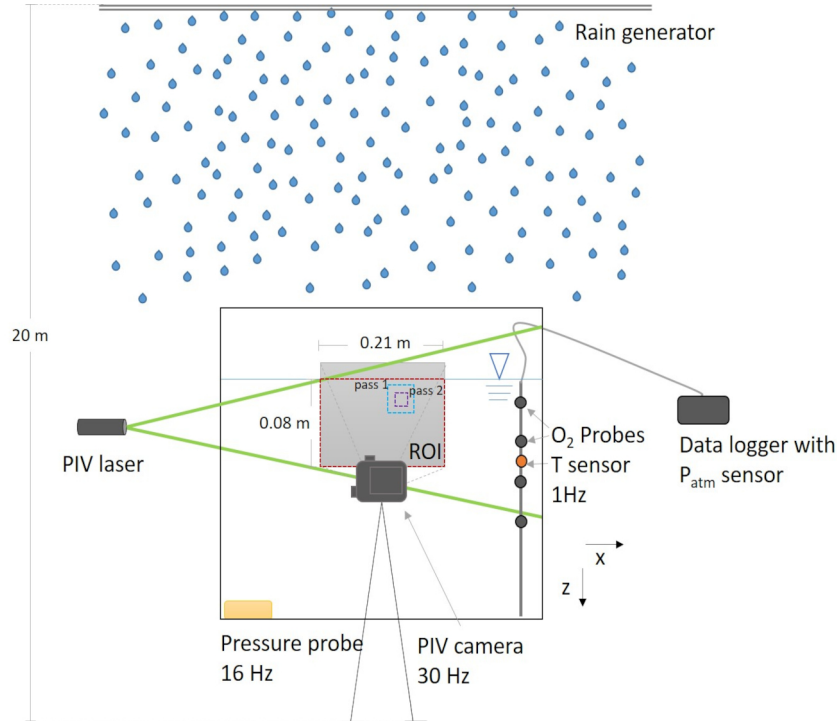


Figure 1. Schematic of the set-up and instrumentation used in the experiments (not to scale). The aquarium ($0.5 \times 0.5 \times 0.5$ m) was located ~ 20 m below the rain generator. Particle image velocimetry (PIV) was used to characterize the turbulent flow field in the water. For this, microscopic seeding particles were illuminated from the side using a laser light sheet, and observed with a camera through the front window. The field of view of the PIV camera (21×12.5 cm on average) is shown as the grey rectangle, the region of interest (ROI) of the PIV measurements (21×8 cm on average) is shown in a red dashed line and the interrogation areas are represented in blue (pass 1) and purple (pass 2) dashed lines. Four sensors for dissolved oxygen (O_2 probes) were used for establishing an oxygen mass balance in the aquarium to estimate the gas transfer velocity. A pressure sensor located at the bottom of the aquarium was used to estimate rain rate from the temporal increase in water level. Atmospheric pressure (P_{atm}) was recorded by the oxygen and temperature data logger.

2.3 Fall velocity, drop sizes and kinetic energy flux of raindrops

The final fall velocity and sizes of raindrops were estimated by placing a planar light at the location in the aquarium and taking videos of the falling raindrops between the light and the camera (backlight illumination). The videos were recorded with a Sony RX100 IV camera at a frame rate of 1000 fps and a resolution of 1920×1080 pixels. A short video of a calibration target was recorded using the same settings. For estimating fall velocity, the recorded

videos were overlaid the image of the calibration target and the number of frames that individual drops could be observed were counted, along with the vertical distance they travelled. Estimates of drop sizes were only performed for a plate configuration with open holes of 0.8 mm.

The kinetic energy flux of the rain (F_{KE} , in $\text{J m}^{-2} \text{s}^{-1}$) was calculated according to the expression proposed by Ho et al. (1997) as follows:

$$\underline{\underline{F_{\text{KE}} = \frac{1}{2} \rho V^2 R}} \quad (1)$$

where ρ is the water density, V is the average fall velocity of the drops and R is rain rate (converted to m s^{-1}).

2.4 Gas transfer velocity

Estimates of the gas transfer velocity of oxygen (k_{O_2}) were obtained from dissolved oxygen (O_2) profiles, following a mass balance approach. We assumed that diffusive exchange with the atmosphere and oxygen transported in rain water as the dominant processes, hence the total rate of change of dissolved oxygen concentration in the aquarium was equated to the sum of the diffusive flux at the water surface (F_{dif}) and the oxygen flux from rain (F_{rain}). Solving for the diffusive flux as follows:

$$\underline{\underline{F_{\text{dif}} = F_{\text{total}} - F_{\text{rain}}}} \quad (2)$$

The total flux (F_{total} , in $\text{mmol m}^2 \text{d}^{-1}$) was calculated for each run from the depth-integrated rate of change of O_2 concentration observed by the four probes as follows:

$$\underline{\underline{F_{\text{total}} = \sum_{i=1}^4 \frac{dC_i}{dt} h_i}} \quad (3)$$

where $\frac{dC_i}{dt}$ is the mean rate of change of dissolved O_2 concentration measured by each O_2 probe (in $\mu\text{mol L}^{-1} \text{d}^{-1}$) and h_i is the representative layer thickness for each sampling depth (in m).

We assumed that the rainwater is saturated with oxygen at the same temperature as the aquarium water, then the oxygen flux associated with rain (F_{rain} , in $\text{mmol m}^2 \text{d}^{-1}$) in the aquarium was as follows:

$$\underline{\underline{F_{\text{rain}} = RC_{\text{eq}}}} \quad (4)$$

where C_{eq} is the O_2 concentration in equilibrium with the atmosphere at given water temperature (in mmol L^{-1}) (Chapra, 1997), and R was converted to volumetric units ($\text{mm h}^{-1} = \text{L h}^{-1}$).

The gas transfer velocity of oxygen at in-situ temperature (k_{O_2} , in m d^{-1}) was estimated using Fick’s first Law as follows:

$$\underline{\underline{k_{\text{O}_2} = \frac{F_{\text{diff}}}{(C_w - C_{\text{eq}})} \quad (5)}}$$

where C_w is the temporarily averaged O_2 concentration measured by the uppermost sensor (in mmol L^{-1}). k_{O_2} was normalized to k_{600} , the gas transfer velocity of CO_2 at 20°C as follows:

$$\underline{\underline{k_{600} = k_{\text{O}_2} \left(\frac{600}{\text{Sc}_{\text{O}_2, T}} \right)^{-n} \quad (6)}}$$

where Sc_{O_2} is the temperature-dependent Schmidt number of oxygen (calculated according to (Raymond et al., 2012) ($\text{Sc}_{\text{O}_2} = \eta / D_{\text{O}_2}$, with η being the viscosity of water and D_{O_2} the diffusion coefficient of oxygen in water). We used the recommended exponent for wavy surfaces ($n = 0.5$) (Jähne et al., 1987).

2.5 Particle image velocimetry

We extracted frame sequences (in bitmap format) from each video that were subsequently converted to greyscale images. The pre-preprocessing of the image sequences and PIV analyses were performed using the open source program PIVlab (v. 2.50) (Thielicke & Sonntag, 2021; Thielicke & Stamhuis, 2014). The imported images were first preprocessed to increase and to homogenize the contrast and sharpness of the laser-illuminated seeding particles, and to remove the image background. The default PIVlab options were chosen: Contrast-limited adaptive histogram equalization (CLAHE) with window size of 20 pixels, highpass filter with a kernel size of 15 pixels, contrast-stretching and background subtraction. The region of interest (ROI) for PIV analysis was selected from the water surface to the maximum resolved depth (Figure 1). One frame of the calibration video was used for conversion from pixels to metric units, with pixel size varying between 0.11 and 0.13 mm among experimental series. Direct Fourier transform correlation with multiple passes and deforming windows was selected as the PIV algorithm and two passes with 50% step size were used, starting with an interrogation area of 128 pixels and decreased to 64 pixels. The final resolution of velocity vectors was 3.9 ± 0.2 mm. Detailed information about filters and processing options can be found in (Thielicke & Sonntag, 2021).

The PIV analysis provided two-dimensional velocity distributions with 3.7 mm spacing for $n \sim 5400$ time steps (corresponding to the total number of frames

in each video of ~3 min duration and recorded at 30 fps). The two resolved velocity components (horizontal velocity u and vertical w) were despiked using a modified phase-space method (Goring & Nikora, 2002). Mean values of the velocity components (\bar{u} and \bar{w}) were calculated as the time-average for each cell the velocity fields (in m s^{-1}). Turbulent velocity fluctuations were calculated based on Reynolds decomposition by subtracting the mean velocities from the instantaneous flow velocities as follows:

$$\overline{u' = u - \bar{u}} \quad (7)$$

$$\overline{w' = w - \bar{w}} \quad (8)$$

2.6 Dissipation rates of turbulent kinetic energy

Viscous energy dissipation rates of turbulent kinetic energy (ϵ) result from velocity gradients along all three spatial dimensions. We used a “direct” estimate of the dissipation rates from the four components of the velocity gradients that are resolved in two-dimensional PIV measurements. According to the expression in Doron et al. (2001), turbulent dissipation rates were calculated (in W kg^{-1} or $\text{m}^2 \text{s}^3$) as follows:

$$\epsilon = 3\nu \left[\left(\frac{\partial u'}{\partial x} \right)^2 + \left(\frac{\partial w'}{\partial z} \right)^2 + \left(\frac{\partial u'}{\partial z} \right)^2 + \left(\frac{\partial w'}{\partial x} \right)^2 + 2 \left(\frac{\partial u'}{\partial z} \frac{\partial w'}{\partial x} \right) + \frac{2}{3} \left(\frac{\partial u'}{\partial x} \frac{\partial w'}{\partial z} \right) \right] \quad (9)$$

where x and y denote horizontal (u) and vertical (w) coordinates. Kinematic viscosity (ν) was in $\text{m}^2 \text{s}^{-1}$. Time-average values of the two-dimensional distributions of dissipation rates (ϵ_{t_avg}) were calculated as averages of log-transformed values (Baker & Gibson, 1987).

Dissipation rates were calculated for all rain experiments, as well as for the measurements without rain. The latter were considered as background turbulence caused by other mechanisms than rain (e.g. convective turbulence), and were subtracted from the final ϵ_{t_avg} results. Finally, dissipation rates were log-averaged horizontally to obtain a mean vertical profile of the turbulent dissipation rate (ϵ_z) for each run.

As near-surface dissipation rate from wind shear stress have been shown to follow a universal power-law decline with increasing depth (Wüest & Lorke, 2003), we tested a power-law approach for describing the vertical attenuation of rain-generated turbulence in the following:

$$\overline{\epsilon_z = a (R)z^{-b}} \quad (10)$$

For all runs, dissipation rate profiles were fitted to equation (10) to obtain

a common exponent b , and a function that describes the dependence of the coefficient a on the rain rate (R). Thus, an empirical function $\epsilon = f(z, R)$ was obtained with ϵ in W kg^{-1} , z in m and R in mm h^{-1} .

In order to explore a mechanistic approach for modeling the gas transfer velocity (k , in m s^{-1}) that represents the response to rain-induced turbulence, a scaling of the turbulent dissipation rate as a function of the rain rate was combined with the surface renewal model (equation (11)) (Lamont & Scott, 1970) as follows:

$$\underline{\underline{k = A \text{Sc}^{-n} (\epsilon v)^{0.25}} \quad (11)}$$

To estimate the dimensionless empirical coefficient A , linear regressions were made between the measured values of k_{600} and the expression $600^{-n} (\epsilon v)^{0.25}$. The regressions were made for dissipation rates measured at the same depth, which we obtained by interpolation of the mean vertical profiles (ϵ_z) between 0.5 to 7.5 cm depth and with a vertical resolution of 0.5 cm. Interpolated profiles were computed for no-rain periods to obtain the background dissipation rates (ϵ_{Back}), as well as for the rain periods (ϵ_{Total}). The dissipation rates resulting from rain (ϵ_{Rain}) was estimated as follows:

$$\underline{\underline{\epsilon_{\text{Rain}} = \epsilon_{\text{Total}} - \epsilon_{\text{Back}}}} \quad (12)$$

Then, we analyzed the dependence of the gas transfer velocity on rain rate (R) and, obtained 15 linear regressions corresponding to different depths at which dissipation rates were measured ($z_1 = 0.5 \text{ cm}$, $z_2 = 1.0 \text{ cm}$,... $z_{15} = 7.5 \text{ cm}$). The quality of the correlations was assessed using the coefficient of determination (r^2), and the best correlation was selected for the final model (k_{600_mod}) by replacing ϵ_{Rain} in equation (11) by the function $\epsilon = f(z, R)$.

3 Results

3.1 Overview

The different configurations of the rain generator resulted in rain rates between 6.9 and 88.9 mm h^{-1} , (Table 1). For the series corresponding to 10.3 and 13.5 mm h^{-1} , the PIV processing for background dissipation rates (no rain) was erroneous due to poor image quality and both k_{600} and dissipation rates obtained at a rain rate of 16.0 mm h^{-1} presented outliers in all subsequent analyses (Table 1). All three runs were excluded from the following analyses of dissipation rates and the 16.0 mm h^{-1} run was also excluded from k_{600} analysis.

@ >p(- 0) * @

Table 1. Summary of experimental results. R is the rain rate, T is the water temperature and Sc_{O_2} is the Schmidt number of oxygen at temperature T . ϵ_{Back} ,

ϵ_{Total} and ϵ_{Rain} are the background (estimated during no-rain periods), the total (estimated during rain), and the rain-induced turbulent dissipation rates, respectively, estimated at 6.5 cm depth. k_{600_Back} , k_{600} and k_{600_mod} are the background (estimated during no rain periods), total (estimated during rain) and the model-predicted gas transfer velocities (equation (15)), respectively. F_{KE} is the estimated kinetic energy flux of rain. Note that ϵ_{Back} and ϵ_{Rain} for rain rates of 10.3 and 13.5 mm h⁻¹ could not be determined (ND) due to poor video quality in the measurements without rain.

@ >p(- 22) * @ Run & R & T & Sc_{O₂} & ϵ_{Back}

[W kg⁻¹] & ϵ_{Total}

[W kg⁻¹] & ϵ_{Rain}

[W kg⁻¹] & $\frac{\epsilon_{\text{Rain}}}{\epsilon_{\text{Total}}}$ & k_{600_Back}

[cm h⁻¹] & k_{600}

[cm h⁻¹] & k_{600_mod}

[cm h⁻¹] & F_{KE}

[W m⁻²]

& 6.90 & 16.9 ± 0.054 & 623 & 1.3 × 10⁻⁸ & 2.4 × 10⁻⁸ & 1.1 × 10⁻⁸ & 44% & 0.820 & 2.99 & 11.2 & 0.0667

2 & 8.05 & 17.1 ± 0.055 & 615 & 1.3 × 10⁻⁸ & 3.0 × 10⁻⁸ & 1.6 × 10⁻⁸ & 55% & 0.820 & 6.97 & 12.0 & 0.0775

3 & 10.3 & 9.48 ± 0.030 & 927 & ND & 3.2 × 10⁻⁸ & ND & ND & -0.058 & 8.29 & 14.4 & 0.0992

4 & 13.5 & 9.35 ± 0.027 & 933 & ND & 8.1 × 10⁻⁸ & ND & ND & -0.058 & 22.0 & 16.5 & 0.130

5 & 16.0 & 9.13 ± 0.737 & 945 & 1.1 × 10⁻⁸ & 1.1 × 10⁻⁷ & 9.5 × 10⁻⁸* & 90% & 4.295 & 48.2* & 18.0 & 0.154

6 & 16.2 & 8.59 ± 0.020 & 973 & 5.8 × 10⁻⁹ & 1.0 × 10⁻⁷ & 2.5 × 10⁻⁸ & 81% & 0.202 & 28.2 & 20.8 & 0.211

7 & 21.1 & 8.36 ± 0.016 & 979 & 5.8 × 10⁻⁹ & 3.0 × 10⁻⁸ & 9.8 × 10⁻⁸ & 94% & 0.202 & 15.6 & 18.2 & 0.168

8 & 19.8 & 8.49 ± 0.021 & 986 & 5.8 × 10⁻⁹ & 2.4 × 10⁻⁷ & 2.3 × 10⁻⁷ & 98% & 0.202 & 16.7 & 20.1 & 0.227

9 & 25.0 & 16.8 ± 0.062 & 624 & 7.5 × 10⁻⁹ & 7.6 × 10⁻⁸ & 6.8 × 10⁻⁸ & 90% & -0.639 & 18.0 & 21.4 & 0.241

10 & 26.0 & 11.0 ± 0.010 & 852 & 6.9 × 10⁻⁹ & 7.6 × 10⁻⁸ & 6.9 × 10⁻⁸ & 91% & 3.632 & 25.6 & 22.7 & 0.250

11 & 28.8 & 17.4 ± 0.087 & 607 & 7.5 × 10⁻⁹ & 9.8 × 10⁻⁸ & 9.1 × 10⁻⁸ & 92% & -0.639 & 19.3 & 22.9 & 0.277

12 & 39.4 & 11.1 ± 0.013 & 849 & 6.9 × 10⁻⁹ & 3.1 × 10⁻⁷ & 3.1 × 10⁻⁷ & 98%

& 3.632 & 30.3 & 28.0 & 0.380
 13 & 48.9 & 17.8 \pm 0.146 & 593 & 7.5×10^{-9} & 2.7×10^{-7} & 2.6×10^{-7} & 97%
 & -0.639 & 25.3 & 29.9 & 0.471
 14 & 88.9 & 18.5 \pm 0.220 & 572 & 7.5×10^{-9} & 3.8×10^{-7} & 3.7×10^{-7} & 98%
 & -0.639 & 46.5 & 40.3 & 0.856

* marks an outlier that caused the run with 16 mm h⁻¹ to be excluded from the subsequent analysis

In the absence of rain, the oxygen concentration in the aquarium did not change significantly, resulting in small gas transfer velocities (-0.79 ± 1.73 cm h⁻¹) (Table 1). During all experiments with rain, the dissolved oxygen concentrations increased nearly linearly with time ($r^2 > 0.90$ for most of the measurements), with similar rates at all sampling depths and with increasing slopes for increasing rain rates (Figure S4). The in-situ gas transfer velocity k_{O_2} was strongly correlated with the rain rate ($r^2 = 0.95$) (Figure 2a). In contrast, the normalized gas transfer velocity (k_{600}), which ranged from 2.99 to 46.5 cm h⁻¹ (Table 1), showed a moderate correlation with the rain rate when all data were included ($r^2 = 0.78$) (Figure 2b).

@ >p(- 0) * @

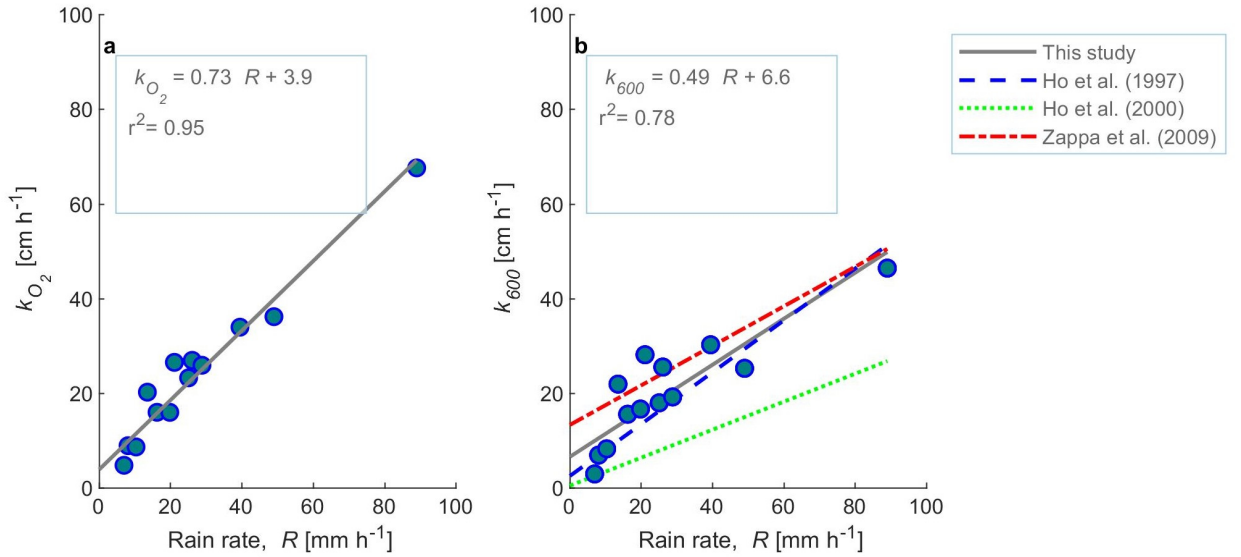


Figure 2. Gas transfer velocity versus rain rate (R) with the linear regressions (solid lines) and the resulting r^2

3.2 Energy dissipation rates

Time-averaged turbulent dissipation rates (ϵ_{t_avg}) were homogeneously distributed along the horizontal direction, but showed strong vertical gradients (Figure S5). They were largest near the water surface and decreased by about two orders of magnitude toward the lower part of the field of view at ~ 7 cm depth. Higher rain rates were associated with higher energy dissipation rates. Thus, ϵ_{t_avg} varied vertically between $\sim 10^{-5}$ and $\sim 10^{-7}$ W kg $^{-1}$ for rain rates R < 25 mm h $^{-1}$, and from $\sim 10^{-4}$ to $\sim 10^{-6}$ W kg $^{-1}$ for $R > 25$ mm h $^{-1}$.

Background dissipation rates measured in the absence of rain, varied between 5.8×10^{-9} and 1.4×10^{-8} W kg $^{-1}$. At a depth of $z = 6.5$ cm, the dissipation rates caused by rain represented 44% to 98% of the total dissipation rate at the lowest and highest evaluated rain rate, respectively (Table 1).

The depth dependence of mean turbulent dissipation rates after background subtraction (ϵ_{Rain}) could be well described by power-law functions for all investigated rain rates ($r^2 = 0.98$, Figure S6). The exponent b (equation (10)) was relatively constant for all rain rates ($b = 2.15 \pm 0.22$ mean \pm std.). The coefficient a in equation (10) was related to the rain rate by a power-law function with an exponent of 2.02 ($r^2 = 0.81$, Figure 3a). Combining both relationships resulted in the following empirical scaling of the dissipation rate (ϵ_{model} in W kg $^{-1}$) as a function of the rain rate (R in mm h $^{-1}$) and depth (z in m):

$$\epsilon_{\text{model}}(R, z) = 4.07 \times 10^{-13} R^{2.02} z^{-2.15} \quad (13)$$

In general, modeled and measured dissipation rates were in good agreement (Figure 3b). Particularly the decline of dissipation rates by two orders of magnitude over the top most 7 cm of the water column was consistent and well described by the model. The overall model showed best agreement for moderate rain rates around 30 - 40 mm h $^{-1}$, while the magnitude of dissipation rates tended to be underestimated for the lowest rain rates (Figure 3b).

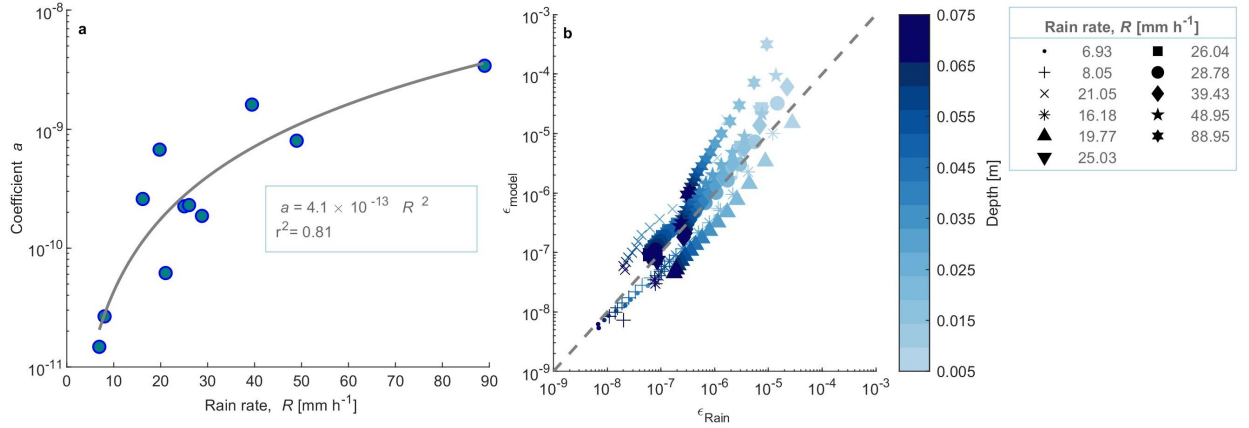


Figure 3. Details of the dissipation rate modeling process **a**) Power-law relationship between the coefficient a (equation (10)) and the rain rate (R) (solid line). **b**) Modeled versus measured dissipation rates for all evaluated rain rates (R) (symbols) and at all evaluated sampling depths (colorbar). The dashed line shows a 1:1 relationship.

3.3 Scaling of the gas transfer velocity

We compared the normalized gas transfer velocities (k_{600}) observed at different rain rates ($n = 14$) against those predicted from turbulent dissipation rates by the surface renewal model (equation (11)). The empirical coefficient A in the surface renewal model was estimated separately for all sampling depth of dissipation rates by linear regression (Figure S7). The correlations were systematically weaker near the water surface ($r^2 \sim 0.50$), and became stronger toward 5.5 - 6.5 cm depth. The best correlation with measured gas transfer velocities were obtained from dissipation rates measured at 6.5 cm depth ($r^2 = 0.44$), with an estimated value of $A = 2.55$ (Figure 4), such that equation (14) becomes as follows:

$$\underline{\underline{k_{600_mod}[\text{m s}^{-1}] = 2.55 \bullet 600^{-0.5} (\epsilon_{\text{Rain}} v)^{0.25}} \quad (14)}$$

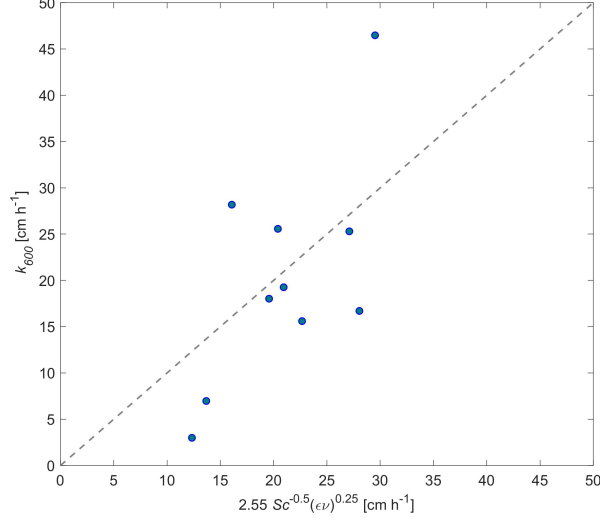


Figure 4. Normalized gas transfer velocities k_{600} versus surface renewal model (Equation (13)) for energy dissipation.

To relate the gas transfer velocity to rain rate (R), we replaced the measured dissipation rate in the surface renewal model by the function (R, z) given in equation (13), to obtain a model of k_{600} (in cm h^{-1}) as a function of the rain rate (R in mm h^{-1}) and kinematic viscosity (ν in $\text{m}^2 \text{s}^{-1}$) as follows:

$$\underline{\underline{k_{600_mod} [\text{cm h}^{-1}] = 130 R^{0.51} \nu^{0.25} \quad (15)}}$$

Gas transfer velocities modeled from rain rates varied from 11.2 to 40.3 cm h^{-1} (Table 1). Good agreement ($r^2 = 0.85$) was found when the model (k_{600_mod}) was linearly correlated with all accepted data of the measured k_{600} (Figure 5).

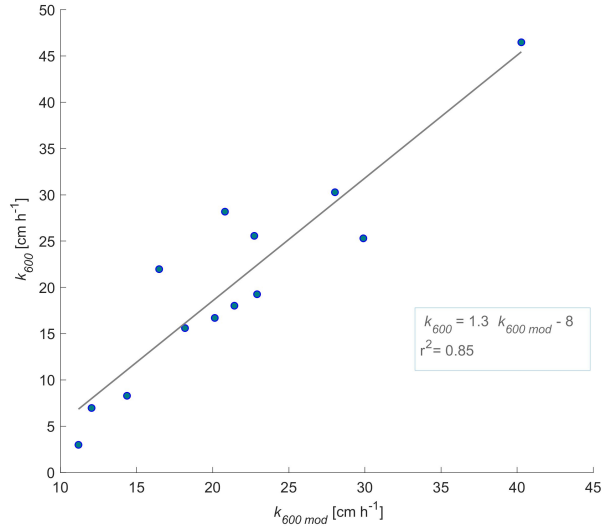


Figure 5. Measured (k_{600}) versus predicted (k_{600_mod}) gas transfer velocities (symbols) and a linear regression (solid line) according to the equation shown in the legend.

3.4 Kinetic energy flux

The fall velocity of the raindrops above the water surface was estimated from observations of 6 individual drops to be $8.3 \pm 2.5 \text{ m s}^{-1}$ (mean \pm std.). The drop size was estimated to be $5.7 \pm 1.1 \text{ mm}$ ($n = 103$). The resulting kinetic energy flux (F_{KE}) ranged from 0.066 to 0.856 W m^{-2} from the lowest to the highest rain rate (Table 1). Following previous studies, we analyzed the relationship between the normalized gas transfer velocity and the kinetic energy flux by fitting a second order polynomial function to k_{600} as a function of F_{KE} (in W m^{-2}) (Figure 6), resulting as follows:

$$k_{600} [\text{cm h}^{-1}] = -34.5F_{\text{KE}}^2 + 77.4F_{\text{KE}} + 4.0$$

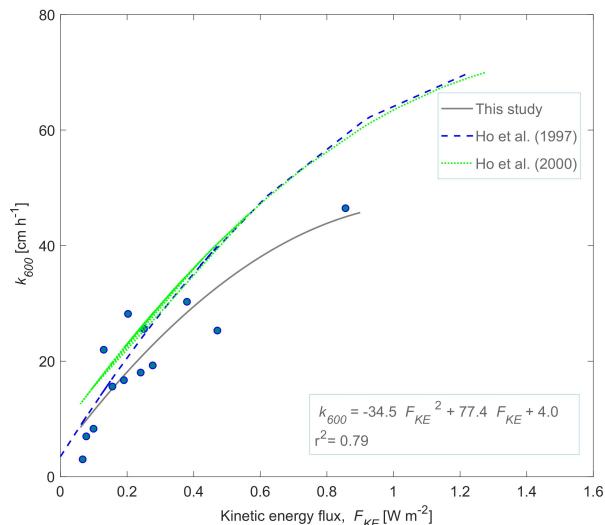


Figure 6. Observed gas transfer velocity (k_{600}) versus kinetic energy flux of rain (F_{KE}). The solid line shows a second-order polynomial fit according to the equation provided in the legend. Dashed lines show corresponding relationships reported in previous studies (Ho et al., 1997, 2000). The data from Ho et al. (1997) were taken from their Table 1 and fitted to a polynomial curve to get the expression $k_{600} = -30.6F_{\text{KE}}^2 + 91.7F_{\text{KE}} + 3.47$ ($r^2 = 0.99$) (Figure S8). The data from Ho (2000) were taken from Figure 8 in Zappa et al. (2009) and the polynomial curve was fitted to get the expression $k_{600} = -26.9F_{\text{KE}}^2 + 84.7F_{\text{KE}} + 5.91$ (Figure S9).

4 Discussion

4.1 Near-surface turbulence

We performed controlled laboratory experiments over a wide range of rain rates combined with robust estimates of spatially-resolved turbulence based on PIV measurements, rain-induced turbulence was characterized.

Our study clearly shows that rainfall enhances both the near-surface turbulence and the gas transfer velocity, in agreement with previous observations (Harrison et al., 2012; Harrison & Veron, 2017; Ho et al., 2004; Takagaki & Komori, 2007; Zappa et al., 2009) (Ho et al., 1997, 2000, 2004; Zappa et al., 2009). Under laboratory conditions and using freshwater, our estimates of the total turbulent dissipation rates (ϵ_{Total}) ranged from 2.43×10^{-8} to 3.77×10^{-7} W kg^{-1} at 6.5 cm depth. These rates were several orders of magnitude smaller than previously reported values, which were around $\sim 10^{-3}$ W kg^{-1} to $\sim 10^{-6}$ W kg^{-1} (Harrison et

al., 2012; Zappa et al., 2009). Such discrepancy could be associated with the consideration of background dissipation rates resulting from other sources than rain, which we subtracted from the measured values to estimate rain-induced turbulence. While our background dissipation rates were in the $6 \times 10^{-9} - 10^{-8}$ W kg^{-1} range, the above studies were characterized by high values of background turbulence, which ranged from $\sim 10^{-6}$ to $\sim 10^{-5}$ W kg^{-1} (Harrison et al., 2012; Zappa et al., 2009). Their estimates of total ϵ during rainfall could be biased by a high background level, which is probably linked to residual flows or convective turbulence during their experiments. To better relate with those studies we estimated the relative increase of dissipation rate from background values (no rain) to rain conditions for each run. Our data show an increase of ~ 1 order of magnitude for a rainfall rate around 40 mm h^{-1} , which agrees with the findings of Harrison et al. (2012), who found ~ 1 order of magnitude increase for a rainfall rate of 60 mm h^{-1} , whereas Zappa et al. (2009) found an increase of ~ 2 orders of magnitude for similar rain rates. Another study using saltwater and heavy rainfall (40 to 190 mm h^{-1}) also reported high total dissipation rates of $\sim 10^{-6}$ to $\sim 10^{-5}$ W kg^{-1} , but did not report the values of background dissipation (Harrison et al., 2017).

Beyond the increase in turbulence as a consequence of rainfall, we found first experimental evidence that the turbulent dissipation rate is a function of rain rate, whereas former studies had only found a causal, nonsystematic relationship (Harrison et al., 2012; Zappa et al., 2009).

4.2 Gas transfer velocity and kinetic energy flux

In this study the gas transfer velocities were estimated using oxygen as a cost-effective alternative to the more traditional trace gas approach. The obtained normalized gas transfer velocities (k_{600}) were mostly within the range reported in previous freshwater studies, (Ho et al., 1997, 2000), albeit at the upper end (Harrison et al., 2012; Ho et al., 2004, 2007). Some of the difference could be attributed to the experimental design. For example, Ho et al. (2004) reported k_{600} values on average 2.4 times lower at comparable rain rates as in this study (25 mm h^{-1}). In their saltwater setup, however, the authors noted that density stratification caused by freshwater falling on saltwater might decrease the gas flux in comparison to freshwater. The spatial distribution and rain drop fall speed may also be important factors that explain the contrasting results. Compared to our study, where the entire aquarium surface was impacted by raindrops, raindrops in Ho et al. (2007) only impacted 3% of the total surface area of the flume, which could explain why our k_{600} values were on average 2.5 times higher at comparable rain rates ($\sim 30 \text{ mm h}^{-1}$). In addition, the mean fall velocities of the raindrops in our study (8.3 m s^{-1}), which were generated 20 m above the aquarium, were close to the terminal velocity (Jones et al., 2010), whereas in Harrison et al. (2012) the height of the rain simulator above the flume was only 2.6 m, leading to smaller fall velocities around 3.13 m s^{-1} .

Linear regressions of k_{600} and R showed moderate correlations ($r^2 = 0.78$), in contrast to Ho et al. (1997) who found a stronger correlation ($r^2 > 0.96$) for all

data obtained in their experiment. However, the oxygen gas transfer velocity (k_{O_2}) correlated better with R than the normalized gas transfer coefficient (k_{600}) ($r^2 = 0.95$) and also our estimates of k_{600} showed good agreement with previous studies (Ho et al., 1997; Zappa et al., 2009) (Figure 2b).

The kinetic energy flux (F_{KE}) proposed by Ho et al. (1997) as a good parameter to explain gas exchange, and that has been used in many subsequent studies (Harrison et al., 2012; Ho et al., 2000, 2004; Zappa et al., 2009), was well correlated with the rain-induced gas transfer velocity. The resulting magnitude of the F_{KE} was similar to the values reported by Ho et al. (1997) and by Zappa et al. (2009) (Figure 6). Similar to the k_{600} - R correlation results, the polynomial expression found in this study for k_{600} as a function of F_{KE} was moderate ($r^2 = 0.79$), but the data were in agreement with the empirical fits reported in previous studies (Ho et al., 1997, 2000; Zappa et al., 2009) for $k_{600} < 30 \text{ cm h}^{-1}$ (Figure 6).

4.3 Surface renewal model

In agreement with Zappa et al. (2009), we found a good agreement between observed gas transfer velocities and predictions by the surface renewal model, contributing to the idea of this model as a possibly unified relationship for the air-water interfacial fluxes in response of a range of environmental forcing conditions. However, the large difference between our dissipation rates and values observed by Zappa et al. (2009), result in larger values of the empirical coefficient in the surface renewal model (A), with $A = 2.55$ being six times larger than the value reported by Zappa et al. (2007, 2009) ($A = 0.42$). In a broader evaluation of the coefficient for different wind and density-driven flows, Esters et al. (2017) reports values between 0.18 and 1.5. Therefore, based on the above values of A , our results appear to be too high. However, we consider a higher value of A for rain-generated gas exchange in comparison to turbulence generated by wind, water currents and convective cooling as plausible, since the surface renewal theory is based on turbulent transport of dissolved gas, whereas in the case of rainfall, gas exchange can be additionally enhanced by entrained air bubbles and water droplets expelled into the air. These mechanisms would result in higher rainfall-generated gas exchange compared to other sources of near-surface turbulence at the same dissipation rate. Regarding bubble-enhanced gas exchange, Ho et al. (2000) determined that 0 to 20% of the gas exchange is produced by bubbles and the rest by rain-induced turbulence. Thus, the relatively small contribution of bubbles would not be sufficient to explain the lower value of the coefficient A in their study in comparison to our estimate. In addition, Zappa et al. (2009) pointed out that the number and size of droplets may also influence bubble formation and consequently gas exchange in freshwater, but no conclusions were drawn in this regard. Further experiments are required to understand the mechanisms of enhanced gas exchange by rainfall in freshwater.

The recurrent finding of previous studies is that the turbulent dissipation rate (ϵ_{Rain}) is not a function of the rain rate (R) (Beyá et al., 2011; Harrison et al.,

2012; Zappa et al., 2009). In this study, the experimental results allowed to obtain a consistent scaling, which shows a power-law relationship between ϵ_{Rain} and R (equation (13)). We consider that the wider range of rain rates tested here is the reason for this finding, since former studies were limited to smaller ranges of observed rain rates: 108 and 141 mm h⁻¹ (Beyá et al., 2011); 40, 100 and 190 mm h⁻¹ (Harrison et al., 2012); 24, 30, 40 and 48 mm h⁻¹ (Zappa et al. 2009).

5 Broader implications

Improved understanding of the effect of rainfall on gas exchange is relevant for assessing the role of aquatic ecosystems in greenhouse gas dynamics, such as the emissions of methane, carbon dioxide and nitrous oxide from reservoirs, wetlands and natural lakes. As suggested by Ho et al. (1997, 2000), the effect of rain on air-water gas exchange is probably most important in inland waters, especially in wind-sheltered systems, where wind is no longer the dominant driver of near-surface turbulence. Particularly, in the tropics, rain intensity is the main aspect of seasonal weather changes and low wind speed and high rain intensity and frequency are conditions typically found (Harrison et al., 2012). Therefore, the consideration of the effect of rain on gas exchange can have major implications for greenhouse gas budgets, not only in terms of short-term dynamics during rain events, but also for explaining seasonal variability of air-water gas exchange in tropical inland waters. But also gas exchange in boreal and temperate inland waters (Ojala et al., 2011), and in marine systems (Ho et al., 2004) can be significantly affected by rain.

Mechanistic models of greenhouse gas dynamics and fluxes in aquatic environments are typically based on mass balances, where gas transfer velocities are either obtained from a few solitary measurements, or described as a function of mean wind speed (Donis et al., 2017; Günthel et al., 2019; Santoso et al., 2020). The application of the scaling relationships for the gas transfer velocity as a function of the rain rate presented in this study can be used to assess the importance of short-term drivers, such as rain events, on gas dynamics and biogeochemical cycling in marine and inland waters. With readily available data on rainfall as the only additional boundary condition required, future studies can apply the scaling relationships in coupled hydrodynamic and biogeochemical models for a broad range of different aquatic ecosystems and climatic boundary conditions.

6 Conclusions

For the first time, our experimental results revealed a positive and systematic relationship between rain rate and turbulence at an air-water interface. Rain-induced dissipation rates of turbulent kinetic energy showed a consistent decrease with increasing sampling depth, and a parabolic relationship with rain rate (equation (13)). We used this empirical model to derive a relationship between the gas transfer velocity as a function of rain rate. In combination, the observed relationships showed good agreement with surface renewal theory

(equation (15)), but with a higher value for the associated empirical constant, than those that have been found in former experiments and for other generation mechanisms of near-surface turbulence, including wind. However, according to current knowledge, the enhancement of gas exchange with rainfall cannot be fully explained, so more experiments are needed to understand the mechanisms of enhanced gas exchange with rainfall in freshwater.

The application of the obtained scaling relationships for the interpretation of flux measurements and their implementations in numerical models has the potential to further improve the understanding of the importance of rain on the magnitude and dynamics of gas exchange and greenhouse gas emissions from aquatic ecosystems.

Acknowledgments

This study was partially supported by the German Research Foundation (DFG), project number LO 1150/12-1 (AL) and RO 5921/1-1 (LR). E.B.B. was funded by the following programs: Scholarship Program No. 757 - National Doctorates of the Ministry of Science, Technology and Innovation of Colombia; Research Grants - Short-Term Grants, 2019 (57440917) of the German Academic Exchange Service (DAAD), and the Call for Teaching and Student Mobility of 2019-2021 of the Facultad de Minas of the Universidad Nacional de Colombia. Thanks to Christoph Bors and to the team of the Environmental Physics Group of the University of Koblenz-Landau for their valuable support during the experiments. Thanks to the Fire Brigade of Landau, Germany, for allowing us to conduct the experiments at their facilities.

Open Research

Datasets for this research are available in these data citation references: Bohórquez, Eliana; Lorke, Andreas; Rovelli, Lorenzo (2021): Dataset: "Rainfall as a Driver for Near-Surface Turbulence and Air-Water Gas Exchange in Aquatic Systems". figshare. Dataset. <https://doi.org/10.6084/m9.figshare.17693792.v1>, with the license CC BY 4.0.

References

- Baker, M. A., & Gibson, C. H. (1987). Sampling turbulence in the stratified ocean: statistical consequences of strong intermittency. In *J. Phys. Oceanogr.* (Vol. 17, Issues 10, Oct. 1987, pp. 1817–1836). [https://doi.org/10.1175/1520-0485\(1987\)017<1817:stits0>2.0.co;2](https://doi.org/10.1175/1520-0485(1987)017<1817:stits0>2.0.co;2)
- Beyá, J., Peirson, W., & Banner, M. (2011). Rainfall-generated, near-surface turbulence. In S. Komori, W. McGillis, & R. Kurose (Eds.), *Gas transfer at water surfaces 2010* (pp. 90–103). Kyoto University Press 2011. <http://hdl.handle.net/2433/156156>
- Chapra, S. C. (1997). *Surface Water-Quality Modeling* (B. J. Clark, D. A. Damstra, & J. W. Bradley (eds.)). McGraw Hill.
- Cole, J., & Caraco, N. F. (1998). Atmospheric Exchange of Carbon Dioxide in a Low-Wind Oligotrophic Lake Measured by the Addition of SF₆. *Limnology and Oceanography*, 43(4), 647–656. <https://doi.org/10.4319/lo.1998.43.4.0647>
- Donis, D., Flury, S., &

Spangenberg, J. E. (2017). Full-scale evaluation of methane production under oxic conditions in a mesotrophic lake. *Nature Communications*, 8(1661), 1–11. <https://doi.org/10.1038/s41467-017-01648-4>Doron, P., Bertuccioli, L., Katz, J., & Osborn, T. R. (2001). Turbulence characteristics and dissipation estimates in the coastal ocean bottom boundary layer from PIV data. *Journal of Physical Oceanography*, 31(8 PART 1), 2108–2134. [https://doi.org/10.1175/1520-0485\(2001\)031<2108:tcadei>2.0.co;2](https://doi.org/10.1175/1520-0485(2001)031<2108:tcadei>2.0.co;2)Esters, L., Landwehr, S., Sutherland, G., Bell, T. G., Christensen, K. H., Saltzman, E. S., Miller, S. D., & Ward, B. (2017). Parameterizing air-sea gas transfer velocity with dissipation. *Journal of Geophysical Research: Oceans*, 122(4), 3041–3056. <https://doi.org/10.1002/2016JC012088>Goring, D. G., & Nikora, V. I. (2002). Despiking acoustic doppler velocimeter data. *Journal of Hydraulic Engineering*, 128(1), 117–126. [https://doi.org/10.1061/\(ASCE\)0733-9429\(2002\)128:1\(117\)](https://doi.org/10.1061/(ASCE)0733-9429(2002)128:1(117))Guérin, F., Abril, G., Serça, D., Delon, C., Richard, S., Delmas, R., Tremblay, A., & Varfalvy, L. (2007a). Gas transfer velocities of CO₂ and CH₄ in a tropical reservoir and its river downstream. *Journal of Marine Systems*, 66(1–4), 161–172. <https://doi.org/10.1016/j.jmarsys.2006.03.019>Guérin, F., Abril, G., Serça, D., Delon, C., Richard, S., Delmas, R., Tremblay, A., & Varfalvy, L. (2007b). Gas transfer velocities of CO₂ and CH₄ in a tropical reservoir and its river downstream. *Journal of Marine Systems*, 66(1–4), 161–172. <https://doi.org/10.1016/j.jmarsys.2006.03.019>Günthel, M., Donis, D., Kirillin, G., Ionescu, D., Bizic, M., McGinnis, D. F., Grossart, H. P., & Tang, K. W. (2019). Contribution of oxic methane production to surface methane emission in lakes and its global importance. *Nature Communications*, 10(1), 1–10. <https://doi.org/10.1038/s41467-019-13320-0>Guseva, S., Aurela, M., Cortés, A., Kivi, R., Lotsari, E., MacIntyre, S., Mammarella, I., Ojala, A., Stepanenko, V., Uotila, P., Vähä, A., Vesala, T., Wallin, M. B., & A. Lorke. (2021). Variable Physical Drivers of Near-Surface Turbulence in a Regulated River Water Resources Research. *Water Resources Research*, 57, 1–27. <https://doi.org/10.1029/2020WR027939>Harrison, E. L., & Veron, F. (2017). Near-surface turbulence and buoyancy induced by heavy rainfall. *Journal of Fluid Mechanics*, 830, 602–630. <https://doi.org/10.1017/jfm.2017.602>Harrison, E. L., Veron, F., Ho, D. T., Reid, M. C., Orton, P., & McGillis, W. R. (2012). Nonlinear interaction between rain- and wind-induced air-water gas exchange. *Journal of Geophysical Research: Oceans*, 117(3), 1–16. <https://doi.org/10.1029/2011JC007693>Ho, D. T., Asher, W. E., Bliven, L. F., Schlosser, P., & Gordan, E. L. (2000). On mechanisms of rain-induced air-water gas exchange. *Journal of Geophysical Research: Oceans*, 105(C10), 24045–24057. <https://doi.org/10.1029/1999jc000280>Ho, D. T., Bliven, L. F., Wanninkhof, R., & Schlosser, P. (1997). The effect of rain on air-water gas exchange. *Tellus B: Chemical and Physical Meteorology*, 49(2), 149–158. <https://doi.org/10.3402/tellusb.v49i2.15957>Ho, D. T., Engel, V. C., Ferrón, S., Hickman, B., Choi, J., & Harvey, J. W. (2018). On Factors Influencing Air-Water Gas Exchange in Emergent Wetlands. *Journal of Geophysical Research: Biogeosciences*, 123(1), 178–192. <https://doi.org/10.1002/2017JG004299>Ho, D. T., Veron, F., Harrison, E., Bliven, L. F., Scott, N., & McGillis, W.

R. (2007). The combined effect of rain and wind on air-water gas exchange: A feasibility study. *Journal of Marine Systems*, *66*(1–4), 150–160. <https://doi.org/10.1016/j.jmarsys.2006.02.012>

Ho, D. T., Zappa, C. J., McGillis, W. R., Bliven, L. F., Ward, B., Dacey, J. W. H., Schollosser, P., & Hendricks, M. B. (2004). Influence of rain on air-sea gas exchange: Lessons from a model ocean. *Journal of Geophysical Research C: Oceans*, *109*(8). <https://doi.org/10.1029/2003JC001806>

Jähne, B., Münnich, K. O., Bösinger, R., Dutzi, A., Huber, W., & Libner, P. (1987). On the parameters influencing air-water gas exchange. *Journal of Geophysical Research*, *92*(C2), 1937. <https://doi.org/10.1029/JC092iC02p01937>

Jones, B. K., Saylor, J. R., & Testik, F. Y. (2010). *Raindrop Morphodynamics*. Katul, G., & Liu, H. (2017). Multiple mechanisms generate a universal scaling with dissipation for the air-water gas transfer velocity. *Geophysical Research Letters*, *44*, 1–7. <https://doi.org/10.1002/2016GL072256>

Käufer, T., König, J., & Cierpka, C. (2021). Stereoscopic PIV measurements using low-cost action cameras. *Experiments in Fluids*, *62*(3), 1–16. <https://doi.org/10.1007/s00348-020-03110-6>

Lamont, J. C., & Scott, D. S. (1970). An Eddy Cell Model of Mass Transfer into the Surface of a Turbulent Liquid. *AIChE Journal*, *16*(4), 513–519. <https://doi.org/10.1002/aic.690160403>

Lorke, A., & Peeters, F. (2006). Toward a Unified Scaling Relation for Interfacial Fluxes. *Journal of Physical Oceanography*, *36*(5), 955–961. <https://doi.org/10.1175/JPO2903.1>

Ojala, A., Bellido, J. L., Tulonen, T., Kankaala, P., & Huotari, J. (2011). Carbon gas fluxes from a brown-water and a clear-water lake in the boreal zone during a summer with extreme rain events. *Limnology and Oceanography*, *56*(1), 61–76. <https://doi.org/10.4319/lo.2011.56.1.0061>

Peirson, W. L., Beyá, J. F., Banner, M. L., Peral, J. S., & Azarmsa, S. A. (2013). Rain-induced attenuation of deep-water waves. *Journal of Fluid Mechanics*, *724*, 5–35. <https://doi.org/10.1017/jfm.2013.87>

Poindexter, C. M., Baldocchi, D. D., Matthes, J. H., Knox, S. H., & Variano, E. A. (2016). The contribution of an overlooked transport process to a wetland’s methane emissions. *Geophysical Research Letters*, *43*(12), 6276–6284. <https://doi.org/10.1002/2016GL068782>

Rantakari, M., Heiskanen, J., Mammarella, I., Tulonen, T., Linnaluoma, J., Kankaala, P., & Ojala, A. (2015). Different Apparent Gas Exchange Coefficients for CO₂ and CH₄: Comparing a Brown-Water and a Clear-Water Lake in the Boreal Zone during the Whole Growing Season. *Environmental Science and Technology*, *49*(19), 11388–11394. <https://doi.org/10.1021/acs.est.5b01261>

Raymond, P. A., Hartmann, J., Lauerwald, R., Sobek, S., McDonald, C., Hoover, M., Butman, D., Striegl, R., Mayorga, E., Humborg, C., Kortelainen, P., Dürr, H., Meybeck, M., Ciais, P., & Guth, P. (2013). Global carbon dioxide emissions from inland waters. *Nature*, *503*(7476). <https://doi.org/10.1038/nature12760>

Raymond, P. A., Zappa, C. J., Butman, D., Bott, T. L., Potter, J., Mulholland, P., Laursen, A. E., McDowell, W. H., & Newbold, D. (2012). Scaling the gas transfer velocity and hydraulic geometry in streams and small rivers. *Limnology and Oceanography*, *2*, 41–53. <https://doi.org/10.1215/21573689-1597669>

Read, J. S., Hamilton, D. P., Desai, A. R., Rose, K. C., Macintyre, S., Lenters, J.

D., Smyth, R. L., Hanson, P. C., Cole, J. J., Staehr, P. A., Rusak, J. A., Pierson, D. C., Brookes, J. D., Laas, A., & Wu, C. H. (2012). *Lake-size dependency of wind shear and convection as controls on gas exchange*. 39, 1–5. <https://doi.org/10.1029/2012GL051886>

Rooney, G. G., van Lipzig, N., & Thiery, W. (2018). Estimating the effect of rainfall on the surface temperature of a tropical lake. *Hydrology and Earth System Sciences*, 22(12), 6357–6369. <https://doi.org/10.5194/hess-22-6357-2018>

Santoso, A. B., Hamilton, D. P., Schipper, L. A., Ostrovsky, I. S., & Hendy, C. H. (2020). High contribution of methane in greenhouse gas emissions from a eutrophic lake: a mass balance synthesis. *New Zealand Journal of Marine and Freshwater Research*, 0(0), 1–20. <https://doi.org/10.1080/00288330.2020.1798476>

Schlesinger, W. H., & Bernhardt, E. S. (2013). *Biogeochemistry: An Analysis of Global Change*. Academic Press. https://books.google.de/books/about/Biogeochemistry.html?id=533UOWBU3_AC&redir_esc=y

Serino, M. A., Carollo, F. G., & Ferro, V. (2019). Raindrop size distribution and terminal velocity for rainfall erosivity studies . A review. *Journal of Hydrology*, 576(February), 210–228. <https://doi.org/10.1016/j.jhydrol.2019.06.040>

Takagaki, N., & Komori, S. (2007). Effects of rainfall on mass transfer across the air-water interface. *Journal of Geophysical Research: Oceans*, 112(6), 1–11. <https://doi.org/10.1029/2006JC003752>

Thielicke, W., & Sonntag, R. (2021). Particle Image Velocimetry for MATLAB: Accuracy and enhanced algorithms in PIVlab. *Journal of Open Research Software*, 9(June), 1–14. <https://doi.org/10.5334/JORS.334>

Thielicke, W., & Stamhuis, E. J. (2014). PIVlab – Towards User-friendly, Affordable and Accurate Digital Particle Image Velocimetry in MATLAB. *Journal of Open Research Software*, 2. <https://doi.org/10.5334/jors.bl>

Turk, D., Zappa, C. J., Meinen, C. S., Christian, J. R., Ho, D. T., Dickson, A. G., & McGillis, W. R. (2010). Rain impacts on CO₂ exchange in the western equatorial Pacific Ocean. *Geophysical Research Letters*, 37(23), 1–6. <https://doi.org/10.1029/2010GL045520>

Wanninkhof, R. (1992). Relationship between wind speed and gas exchange over the ocean. *Journal of Geophysical Research*, 97(C5), 7373–7382. <https://doi.org/10.1029/92JC00188>

Winter, T. C. (2004). The Hydrology of Lakes. In P. . O’Sullivan & C. S. Reynolds (Eds.), *The Lakes Handbook* (pp. 61–78).

Wüest, A., & Lorke, A. (2003). Small-Scale Hydrodynamics in Lakes. *Annual Reviews of Fluid Mechanics*, 35(Section 3), 373–412. <https://doi.org/10.1146/annurev.fluid.35.101101.161220>

Xu, D., & Chen, J. (2013). Accurate estimate of turbulent dissipation rate using PIV data. *Experimental Thermal and Fluid Science*, 44, 662–672. <https://doi.org/10.1016/j.expthermflusci.2012.09.006>

Zappa, C. J., Ho, D. T., McGillis, W. R., Banner, M. L., Dacey, J. W. H., Bliven, L. F., Ma, B., & Nystuen, J. (2009). Rain-induced turbulence and air-sea gas transfer. *Journal of Geophysical Research: Oceans*, 114(7), 1–17. <https://doi.org/10.1029/2008JC005008>

Zappa, C. J., McGillis, W. R., Raymond, P. A., Edson, J. B., Hints, E. J., Zemmelen, H. J., Dacey, J. W. H., & Ho, D. T. (2007). Environmental turbulent mixing controls on air-water gas exchange in marine and aquatic systems. *Geophysical Research Letters*, 34, 1–6. <https://doi.org/10.1029/2006GL028790>

References From the Supporting Information

Ho, D. T., Asher, W. E., Bliven, L. F., Schlosser, P., & Gordan, E. L. (2000). On mechanisms of rain-induced air-water gas exchange. *Journal of Geophysical Research: Oceans*, 105(C10), 24045–24057. <https://doi.org/10.1029/1999jc000280>

Ho, D. T., Bliven, L. F., Wanninkhof, R., & Schlosser, P. (1997). The effect of rain on air-water gas exchange. *Tellus B: Chemical and Physical Meteorology*, 49(2), 149–158. <https://doi.org/10.3402/tellusb.v49i2.15957>

Zappa, C. J., Ho, D. T., McGillis, W. R., Banner, M. L., Dacey, J. W. H., Bliven, L. F., Ma, B., & Nystuen, J. (2009). Rain-induced turbulence and air-sea gas transfer. *Journal of Geophysical Research: Oceans*, 114(7), 1–17. <https://doi.org/10.1029/2008JC005008>

Figure 1. Schematic of the set-up and instrumentation used in the experiments (not to scale). The aquarium ($0.5 \times 0.5 \times 0.5$ m) was located ~ 20 m below the rain generator. Particle image velocimetry (PIV) was used to characterize the turbulent flow field in the water. For this, microscopic seeding particles were illuminated from the side using a laser light sheet, and observed with a camera through the front window. The field of view of the PIV camera (21×12.5 cm on average) is shown as the grey rectangle, the region of interest (ROI) of the PIV measurements (21×8 cm on average) is shown in a red dashed line and the interrogation areas are represented in blue (pass 1) and purple (pass 2) dashed lines. Four sensors for dissolved oxygen (O_2 probes) were used for establishing an oxygen mass balance in the aquarium to estimate the gas transfer velocity. A pressure sensor located at the bottom of the aquarium was used to estimate rain rate from the temporal increase in water level. Atmospheric pressure (P_{atm}) was recorded by the oxygen and temperature data logger.

Figure 2. Gas transfer velocity versus rain rate (R) with the linear regressions (solid lines) and the resulting equations shown as legends. **a)** gas transfer velocity for oxygen at in situ temperature (k_{O_2}), **b)** Normalized gas transfer velocity (k_{600}) and comparisons to previous studies (dashed lines: (Ho et al., 1997, 2000; Zappa et al., 2009)). The data from Zappa et al. (2009) were taken from their Figure 9 and fitted with a linear regression to obtain the expression $k_{600} = 0.42R + 13.3$ ($r^2 = 0.97$).

Figure 3. Details of the dissipation rate modeling process **a)** Power-law relationship between the coefficient a (equation (10)) and the rain rate (R) (solid line). **b)** Modeled versus measured dissipation rates for all evaluated rain rates (R) (symbols) and at all evaluated sampling depths (colorbar). The dashed line shows a 1:1 relationship.

Figure 4. Normalized gas transfer velocities k_{600} versus surface renewal model (Equation (13)) for energy dissipation rates sampled at $z = 6.5$ cm depth. At this depth, we estimated the value of the coefficient A as 2.55, Sc is the Schmidt number (here equal to 600). The dashed line shows a 1:1 relationship.

Figure 5. Measured (k_{600}) versus predicted (k_{600_mod}) gas transfer velocities

(symbols) and a linear regression (solid line) according to the equation shown in the legend.

Figure 6. Observed gas transfer velocity (k_{600}) versus kinetic energy flux of rain (F_{KE}). The solid line shows a second-order polynomial fit according to the equation provided in the legend. Dashed lines show corresponding relationships reported in previous studies (Ho et al., 1997, 2000). The data from Ho et al. (1997) were taken from their Table 1 and fitted to a polynomial curve to get the expression $k_{600} = -30.6F_{KE}^2 + 91.7F_{KE} + 3.47$ ($r^2 = 0.99$) (Figure S8). The data from Ho (2000) were taken from Figure 8 in Zappa et al. (2009) and the polynomial curve was fitted to get the expression $k_{600} = -26.9F_{KE}^2 + 84.7F_{KE} + 5.91$ (Figure S9).

Table 1. Summary of experimental results. R is the rain rate, T is the water temperature and Sc_{O_2} is the Schmidt number of oxygen at temperature T . ϵ_{Back} , ϵ_{Total} and ϵ_{Rain} are the background (estimated during no-rain periods), the total (estimated during rain), and the rain-induced turbulent dissipation rates, respectively, estimated at 6.5 cm depth. k_{600_Back} , k_{600} and k_{600_mod} are the background (estimated during no rain periods), total (estimated during rain) and the model-predicted gas transfer velocities (equation (15)), respectively. F_{KE} is the estimated kinetic energy flux of rain. Note that ϵ_{Back} and ϵ_{Rain} for rain rates of 10.3 and 13.5 mm h⁻¹ could not be determined (ND) due to poor video quality in the measurements without rain.

Rainfall as a Driver for Near-Surface Turbulence and Air-Water Gas Exchange in Aquatic Systems

Eliana Bohórquez-Bedoya^{1,2,*}, Lorenzo Rovelli², and Andreas Lorke²

¹ Department of Geosciences and Environment, Universidad Nacional de Colombia, Medellín, Colombia.

² Institute for Environmental Sciences, University of Koblenz-Landau, Landau, Germany.

* Corresponding author: Eliana Bohórquez-Bedoya (elibohorquezbed@unal.edu.co)

Contents of this file

Figures S1 to S9

Additional Supporting Information (Files uploaded separately)

None

Introduction

The supporting information provided here consists of images showing the experimental setup and figures with specific results. The figures of the results were processed in Matlab R2021a. No anomalies are presented in the data.

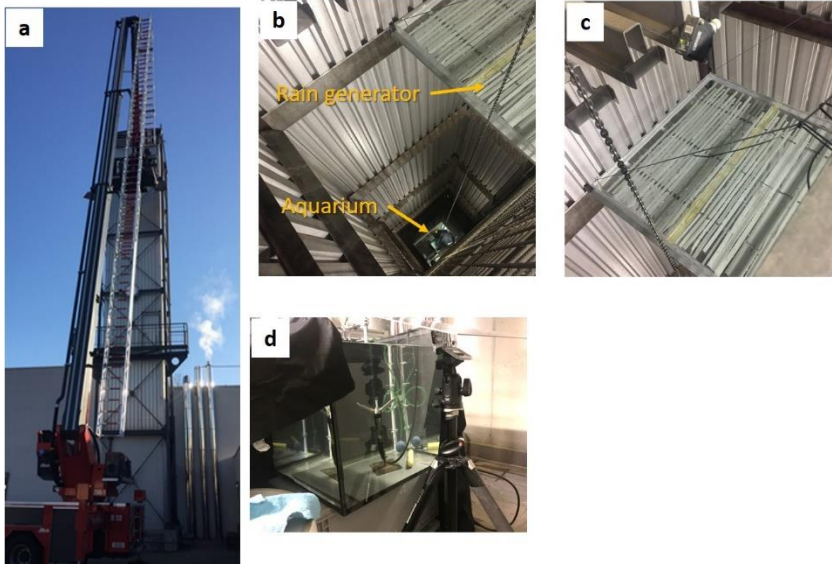


Figure S1. Pictures of the experimental setup: a) Hose-drying tower (approximately 20 m tall) of the municipal fire brigade in Landau, Germany, in which experiments were conducted. b) Inside view showing the rain generator in the top and the aquarium at the base of the tower. c) detailed view of the rain generator (cf. Fig. 1). d) Aquarium with sensors and camera mounting frame.



Figure S2. Picture of the rain generator: The outer aluminum frame (1 x 1 x 0.05 m) was filled with water and raindrops formed at regularly arranged holes in the transparent bottom plate. The rainfall rate was varied by closing or opening a varying number of holes using adhesive tape (visible as black and silver tape stripes in the picture).

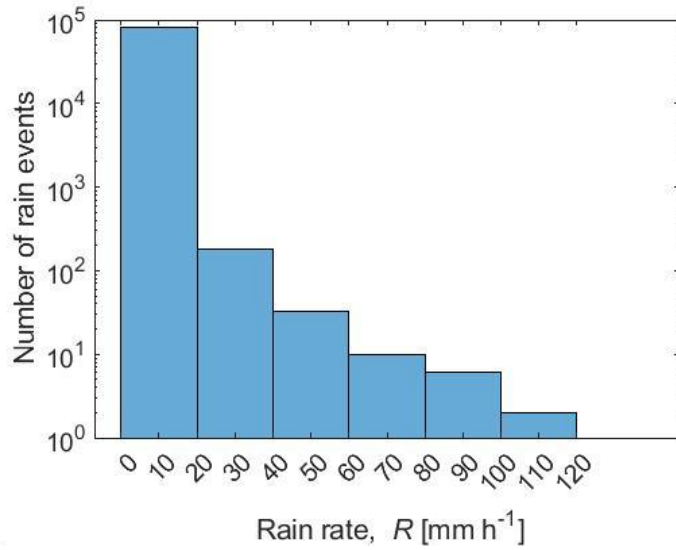


Figure S3. Histogram of local precipitation at Porce III reservoir, Colombia ($6^{\circ}54'12.6''\text{N}$, $75^{\circ}10'16.1''\text{W}$). Data were obtained from measurements with 1h resolution for the period between 1 January 2017 and 1 May 2019 ($n = 81601$).

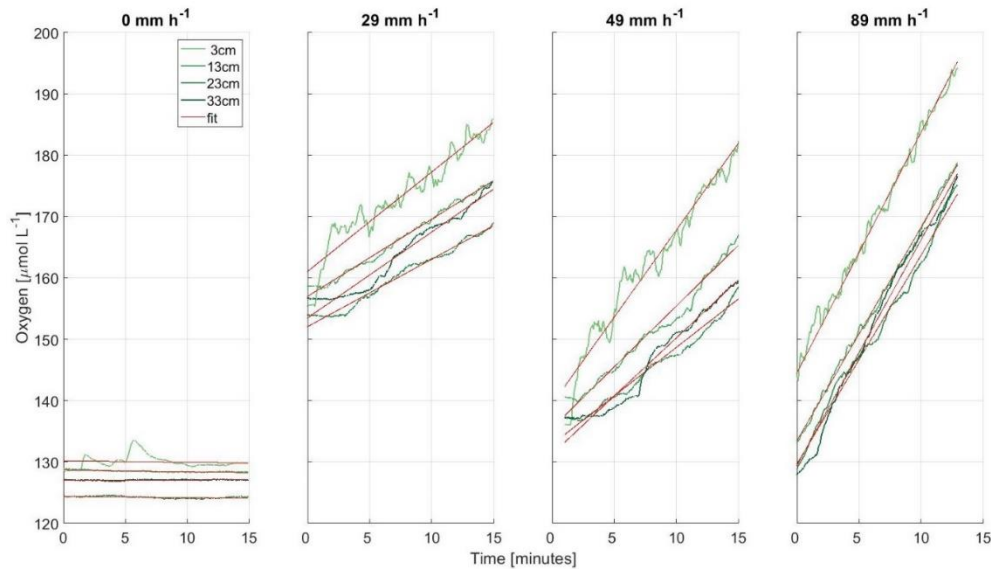


Figure S4. Time series of dissolved oxygen concentration at different sampling depth in the aquarium (line color, see legend) observed without rain and for three different rain rates (see panel headings). Red solid lines show linear regressions that were used for estimating the gas transfer velocity according to Eq. (3).

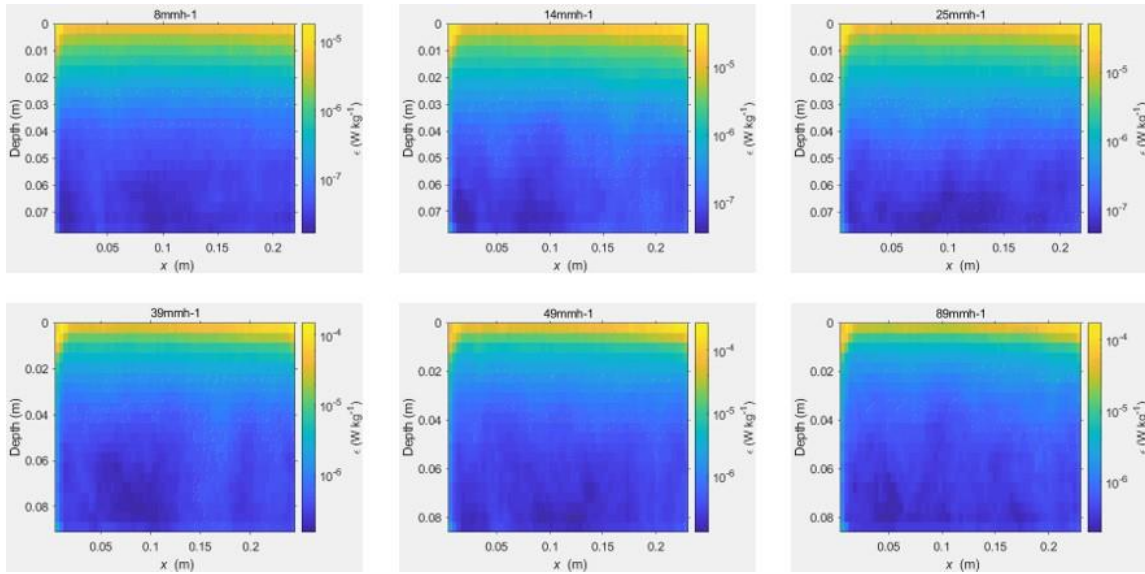


Figure S5. Spatial distribution of the time-averaged turbulent dissipation rates (ϵ_{t_avg}) for six different rain rates (see panel titles).

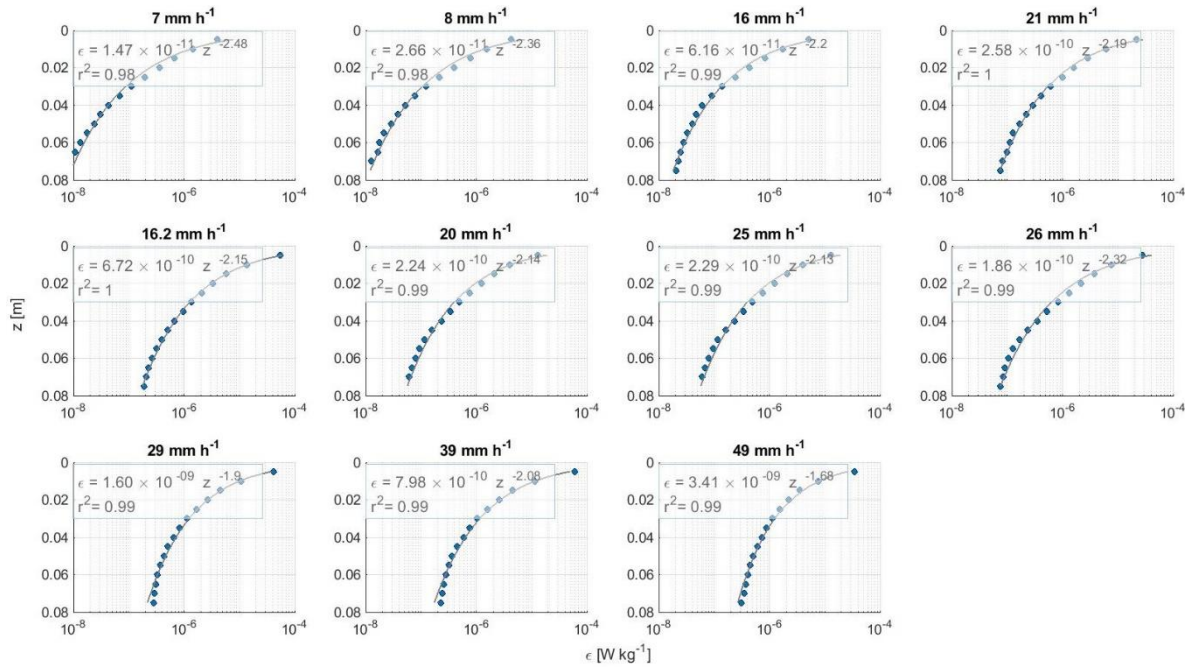


Figure S6. Mean vertical profiles of dissipation rates of turbulent kinetic energy for all measured rain rates (filled symbols). The solid lines show power-law fits according to the function shown in each legend.

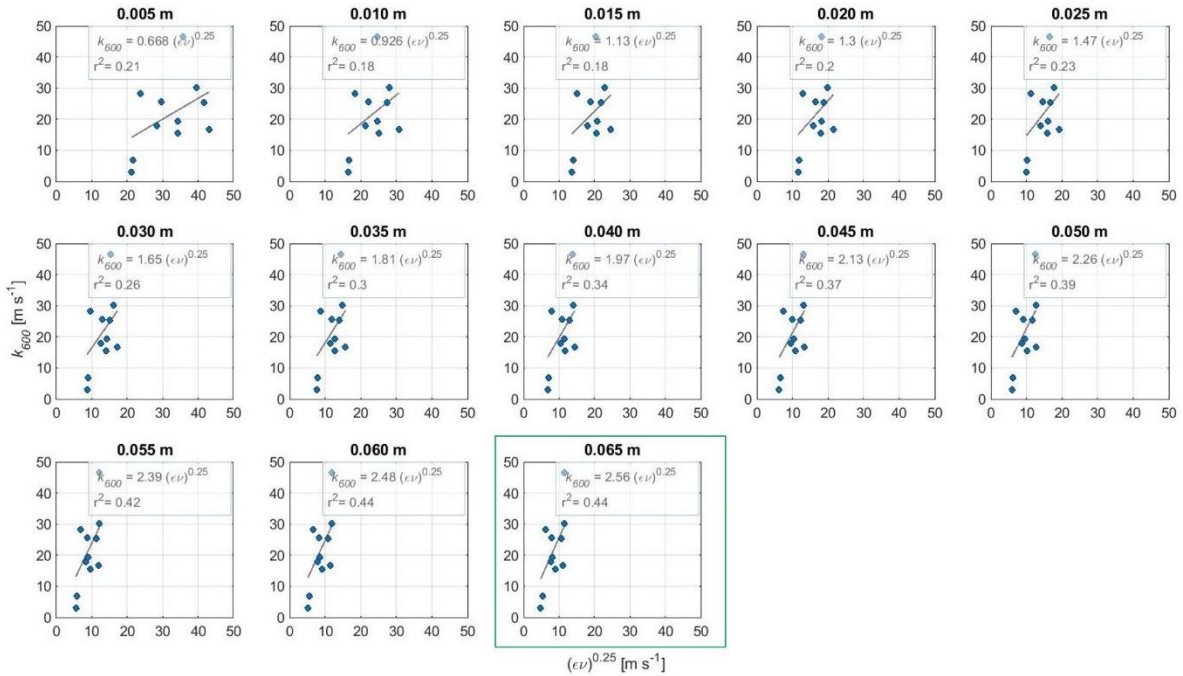


Figure S7. Normalized gas transfer velocities k_{600} versus the surface renewal model (Eq. (13)) for different water depth at which dissipation rates (ϵ) were measured. Solid lines show linear regressions according to the equation shown in the legends. The best fit, which was chosen to estimate the empirical coefficient A is highlighted by the green bounding box.

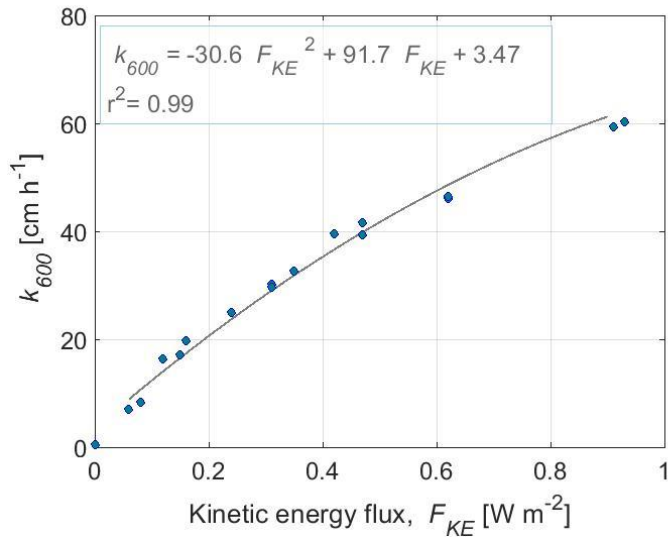


Figure S8. Normalized gas transfer velocity k_{600} as a function of the kinetic energy flux of rain reported in Ho et al. (1997) (their Table 1). The solid line shows a polynomial fit according the equation shown in the legend.

